Cost-effective BRDF spectroscopic bench involving gimbal-based sample positioning system

J. Hastanin *, E. Mazy, L. Clermont, C. Michel, C. Dandumont, M. Georges, L. Rossi, S. Marcotte,
F. Rabecki and C. Thizy

Centre Spatial de Liège (CSL), STAR Research Unit, Université de Liège, Liege Science Park,
Angleur, B-4031, Belgium

ABSTRACT

This paper addresses the engineering aspects of implementing a cost-effective instrumental approach to measuring the Bidirectional Reflectance Distribution Function (BRDF) of optical diffusers. The measurement bench presented involves a PerkinElmer UV/Vis/NIR spectrophotometer equipped with a sample angular orientation system based on a compact motorized gimbal. This instrumental approach allows for measuring the BRDF with accuracy comparable to that achieved in much more expensive robot-based gonioreflectometer benches. Its practical implementation is straightforward and does not require significant costs for purchasing additional measuring equipment or adapting the laboratory clean room. The presented approach can be easily adapted to other available spectrophotometers. Additionally, we introduce a relatively simple yet effective data processing method and discuss various aspects of its practical use for analyzing measurement data obtained using the developed spectrometric bench.

Keywords: BRDF measurement, Total Absolute Measurement System, TAMS spectrophotometers, diffusers calibration

* jhastanin@uliege.be

1. INTRODUCTION

The Bidirectional Reflectance Distribution Function (BRDF) is a multidimensional function that quantifies the amount of light reflected from a diffuse surface, such as paints, bulk substrates, or multi-layer and gradient coatings [1]. A thorough understanding of the BRDF of optical materials and components is essential for optimizing the design of high-quality optical devices and systems used in various applications. For example, some instruments use a diffuser to perform regular in-orbit spectral and radiometric calibration, using the sun as a reference object. Such solar diffusers are used in spectrometers for Earth observation applications, for example, on the Sentinel 1-5 missions [2]-[5]. BRDF characterization is also essential for evaluating the properties of black coatings, used to control the scattering that can occur on the non-optical surfaces of optical instruments [6]-[9]. Finally, BRDF measurements are done to evaluate the scattering effects when light hits an optical surface, as it can impact the resolution of optical instruments [10] or create noise on the detector [11]-[13], including when considering out-of-field sources [14].

BRDF measurements are carried out using dedicated metrology apparatus, the most accurate of which are currently robot-based gonioreflectometers (RG), such as those developed by the National Metrology Institute of Germany, PTB (Physikalisch-Technische Bundesanstalt) [15], and the ROSI (Robotic Optical Scattering Instrument) at NIST (US National Institute of Standards and Technology) [16]. An RG bench has been developed at our institute (CSL) for characterizing large diffusers for on-board radiometric calibration applications [17]. High accuracy has been demonstrated, thanks to an automatic fine positioning of the robotic arm, enabled by an initial laser tracker characterization [18], [19]. The RGs are versatile and meet practically all the requirements for the optical characterization of diffusers. However, it should be noted that metrology instruments of this type and the characterization process of samples using these instruments appear quite expensive, especially for small research laboratories. In addition, these instruments should be placed in large volume clean rooms with high insulation from straylight, which further raises the overall costs and complexity of the measurement system.

Meanwhile, small metrology laboratories often need to measure BRDF quickly on many small and lightweight samples, while slightly reduced measurement accuracy is considered acceptable. For example, this situation frequently arises when optimizing optical surface processing technologies, such as thin film coating, laser micromachining, and chemical etching. Another example includes metrological studies of the ultraviolet (UV) resistance of calibration diffusers, which refers to their ability to withstand degradation caused by UV exposure.

Optical Measurement Systems for Industrial Inspection XIV, edited by Peter Lehmann,
Wolfgang Osten, Armando Albertazzi Gonçalves, Proc. of SPIE Vol. 13567
1356723 · © 2025 SPIE · 0277-786X · doi: 10.1117/12.3059479

In such a case, the following simple strategy appears to be the most logical and economically practical: the accurate measurements involving the high-quality, yet expensive RG bench are performed only at key steps of the fabrication process flow (such as initial and final specimen characterization, etc.) and/or only for specific key measurement configurations (angular or spectral). Meanwhile, intermediate characterization of samples between non-critical process operations can be carried out using inexpensive measuring equipment with conventional optical spectrometers customized for BRDF measurement purposes. The former, costly RG characterization of the samples can be conducted, inter alia, by an external independent metrology laboratory (such as NIST, PTB, CSL, etc.).

In our work, the above-mentioned metrological scenario is implemented using two distinct characterization benches: the CSL RG, for high-precision BRDF measurements [17]-[19], and the UV/Vis/NIR spectrophotometers PerkinElmer LAMBDA™ 950/1050, equipped with a motorized sample holder, also called a "sample positioning system" (SPS), which involves a compact three-axis gimbal for performing quick intermediate relative measurements. We chose an SPS of this type because it is much more compact and less expensive than existing commercial robotic arms, making it better suited for integration into spectrophotometers with rather limited space available for the installation of additional modules.

In this paper, we discuss several aspects of implementing the instrumental approach for BRDF measurements using the spectrometric bench equipped with gimbal-based motorized SPS. This approach is well-suited and primarily dedicated to small research laboratories since its practical implementation does not require significant expenses compared to those needed for developing a RG, especially considering that many such laboratories already have spectrometers of the same (or similar) type as the one used in our work. The two instrumental approaches mentioned are complementary to one another and cannot be explicitly compared in terms of optical quality parameters such as measurement accuracy and precision, which depend on user-defined spectral scan parameters (integration time, wavelength resolution, etc.). One of the main advantages of the measurement bench based on the PerkinElmer LAMBDA™ 950/1050 spectrophotometers, in addition to its relatively low overall cost, is its capability to perform BRDF measurements over a very wide wavelength range: from 175 to 3300 nm. By comparison, the NIST ROSI, PTB, and CSL RG benches allow BRDF measurements over wavelength ranges of 400-2400 nm, 400-1700 nm, and 400-2400 nm, respectively. However, this measurement bench has limitations regarding its functionality. In particular, unlike robot-based benches, it is not suitable for measuring large and heavy samples, nor does it allow measurement of the spatial variation of the BRDF over the sample surface.

In practice, the aforementioned intermediate measurements are often performed for comparative purposes. This means that we are interested not so much in the absolute BRDF value measured for a sample under test, but more in its change caused by variations in the chemical-physical process parameters selected for a given technological operation, while the measurand is the ratio of two BRDFs of the sample taken before and after processing. Additionally, one of the subtasks we frequently encounter when analysing and processing data from intermediate measurements is the extrapolation (interpolation) of BRDF data beyond (within) wavelength ranges for which no data have been obtained using the more precise RG bench. Our experience has shown that in such cases, it is practical to use data processing methods involving preliminary normalization of measurement data (for example, spectral normalization). In this article, we also present a relatively simple but effective data processing method involving spectral normalization and discuss aspects of its practical use for interpolating and extrapolating measurement data obtained using the spectrometric bench equipped with gimbal-based SPS. Finally, it is worth noting that the relatively small size of the specimen chamber of this measuring instrument facilitates measurements in a dry-nitrogen-purged environment, thus preventing the absorption of light by water vapor when measuring in the infrared range.

2. BACKGROUND

The BRDF is defined as the ratio of the directional reflected radiance (*dL*) to the directional incident irradiance (*dE*) and can be calculated as follows, [1], [18]-[19]:

$$BRDF(\theta_i,\phi_i,\theta_r,\phi_r,\lambda)=\frac{dL_r(\theta_i,\phi_i,\theta_r,\phi_r,\lambda)}{dE_i(\theta_i,\phi_i,\lambda)}=\frac{dL_r(\theta_i,\phi_i,\theta_r,\phi_r,\lambda)}{L_i(\theta_i,\phi_i,\lambda)\,d\Omega_r\cos(\theta_i)}\quad\left[sr^{-1}\right] \tag{1}$$

where λ is the wavelength of the incident light, $d\Omega_r$ denotes the solid angle of the detection aperture, θ_i and φ_i are, respectively, elevation and azimuth angles of the incident beam, and θ_r and φ_r the ones of the scattered beam, as illustrated in Fig. 1; dL_r and dE_i denote respectively the differential reflection radiance and the differential incident irradiance.

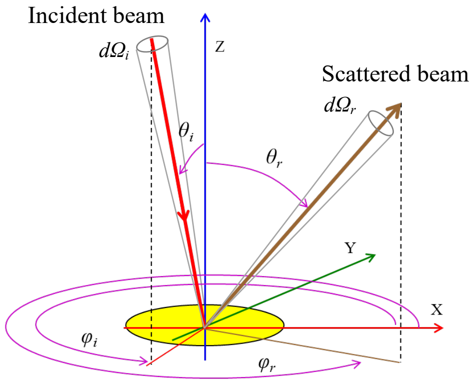

Figure 1. Geometry for the definition of the BRDF

In practice, the differential terms in this equation cannot be measured directly. Instead, the subject of direct measurements is the value of the BRDF averaged over the illuminated surface of the sample viewed within the detector's solid angle of view. This average BRDF is then calculated as follows:

$$\langle BRDF(\theta_i, \varphi_i, \theta_r, \varphi_r, \lambda)\rangle = \frac{S_{scat}(\theta_i, \varphi_i, \theta_r, \varphi_r, \lambda)}{S_{src}} \cdot \frac{1}{d\Omega_r \cos(\theta_i)} \tag{2}$$

In this equation, S_{scat} and S_{src} are respectively the scattering and reference signals measured in the required angular configuration (θi, φi; θr, φr) in the spectral band of interest.

In addition, in the case of the sample comparative characterization involving relative measurement methods, as well as when calibrating a measuring instrument, it is often convenient to investigate obtained measurement results in terms of the relative spectral response function (RSRF), defined as the following ratio:

$$\psi(\theta_i, \varphi_i, \theta_r, \varphi_r, \lambda) = \frac{\langle BRDF(\theta_i, \varphi_i, \theta_r, \varphi_r, \lambda)\rangle}{\langle\langle BRDF(\theta_i, \varphi_i, \theta_r, \varphi_r, \lambda)\rangle\rangle_\lambda} = \frac{S_{scat}(\theta_i, \varphi_i, \theta_r, \varphi_r, \lambda)}{S_{src}} \cdot \left\langle \frac{S_{scat}(\theta_i, \varphi_i, \theta_r, \varphi_r, \lambda)}{S_{src}} \right\rangle_\lambda^{-1} \tag{3}$$

where $\langle\langle BRDF(\theta_i, \varphi_i; \theta_r, \varphi_r, \lambda)\rangle\rangle_\lambda$ is averaged spectral value of the measured BRDF.

3. MEASUREMENT BENCH DESIGN AND OPERATION PRINCIPLE

3.1 Proof-of-concept prototype

The first proof-of-concept prototype of the gimbal-based SPS, utilized in our experimental work to investigate the functionality and performance of the proposed instrumental approach, was developed based on the 'Total Absolute Measurement System' (TAMS) accessory module manufactured by "OMT Solutions" (www.omtsolutions.com) for spectrophotometers of the PerkinElmer LAMBDA™ 950/1050 series.

Fig. 2 shows the mechanical layout of the TAMS module. From a functional perspective, the investigated BRDF measurement bench features a relatively simple design, consisting of a UV/Vis/NIR spectrophotometer (1) used as a radiation source with a tunable wavelength, as well as for the primary processing of the detected signal, and the TAMS module designed to position the sample (2) and detector (3) at angular positions corresponding to the required measurement configuration (θi, φi; θr, φr). The TAMS module can be functionally divided into two independent parts: a detector assembly and the sample holder. The detector is mounted on a motorized rotation ring that moves it around the fixed vertical axis Y. It is important to note that the sample holder assembly represents an insertable module built according to a modular concept and can be equipped with either one (Fig. 2a) or two (Fig. 2b) motorized rotation stages, depending on the user's preference.

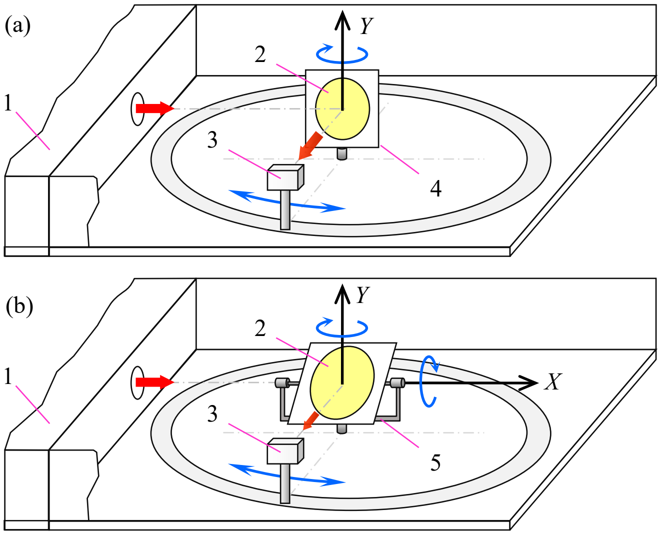

Figure 2. Mechanical layout of the TAMS module in the simplified basic version of the design (a) and in the advanced one (b) equipped with a two-axis gimbal sample holder.

The baseline specifications for the TAMS module are summarized in Table 1.

Table 1. Global design specifications of TAMS

Wavelength range	190-3300 nm
Spot size	8×9 mm (max)
Maximum size sample	200 mm×180 mm
Sample to detector distance	0.115 m
Sample angle	-180°…+180°; resolution: 0.01°; accuracy: 0.02°
Detector angle	15°…345°; resolution: 0.01°; accuracy: 0.02°
Angle range reflexion	7.5°…+/-80°

It is instructive to note that the basic, less expensive version of the TAMS module (Fig.2a), which involves only one motorized rotation platform (4), allows for measurements of the sample BRDF only in specific cases where both the incident and scattered beams are in the plane normal to the sample. This means in-plane measurements (i.e., when in the required angular configuration: $\varphi i = \varphi r \pm \pi$).

The model of the TAMS used in our work (Fig.2b) is equipped with a motorized two-axis gimbal (5).

In the case of the TAMS-based spectroscopic setup, the BRDF measurement procedure is similar to that used for the RG bench and involves two consecutive measurements: the reference and scattered beam measurements. During the reference measurement, the sample holder assembly is removed from the TAMS module, and the detector is positioned in front of the incident light beam (in other words, in front of the exit window of the spectrophotometer). To measure the scattered beam power, the sample holder is reinstalled in the TAMS module in its initial position. Then, the sample and detector are adjusted from the initial to the required angular configuration using the corresponding motorized rotation stages. The BRDF value is calculated by substituting the measured values of the reference and scattered signals in Eq. (2).

The set of input angles (θi, φi; θr, φr) defining the required measurement configuration specifies the directions of the incident and scattered beams relative to the local reference frame S1, which is connected to the sample fixed in the motorized sample holder, as shown in Fig.3. Furthermore, it determines the angle ξ between the light probe beam emitted by the spectrometer and the direction of detection in the laboratory reference frame S0 (fixed relative to the TAMS). In our work, the sample's initial position is assumed to correspond to the normal incidence of the probe beam on its surface.

As noted above, the sample holder assembly of the TAMS used in our work is equipped with only two motorized rotation stages (two-axis gimbal): one for rotation around the vertical axis Y and one for rotation around an axis X parallel to the sample surface (Fig. 2b). However, according to Euler's rotation theorem, to achieve a rotation around an arbitrarily oriented axis in space, i.e., to enable BRDF measurements in an arbitrary angular configuration (θi, φi; θr, φr), at least three degrees of rotational freedom are required. In other words, the sample holder module must be equipped with at least three linearly independent rotation stages. Accordingly, an additional degree of freedom must be integrated into the mechanical system of the sample holder assembly: the rotation of the sample around the axis orthogonal to its surface (denoted as θz in Fig. 3). In our measurement bench, an additional homemade non-motorized rotation stage provides this degree of freedom. However, other commercially available standard rotation stages can also be adapted for this purpose.

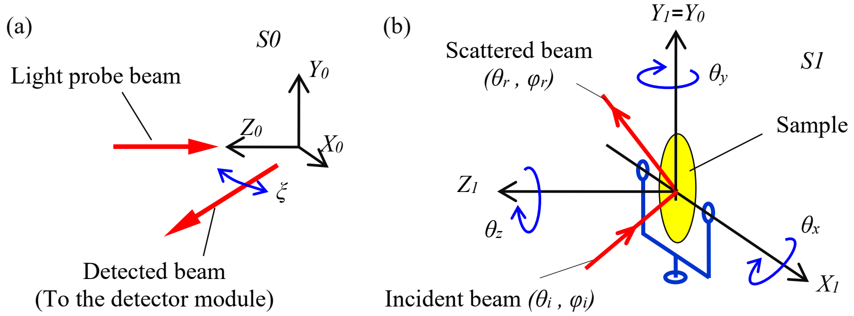

Figure 3. Lighting and detection configuration diagram in the laboratory reference frame S0 (a) and schematic diagram of the incident and scattering configuration in the sample holder reference frame S1 (b)

Finally, it is worth noting that in reference frame S1, only the Z1-axis is intrinsic, i.e., the body-fixed (physically attached to the sample). The vertical Y1 axis is fixed with respect to the laboratory reference frame. The X-axis remains horizontal and parallel to the plane of the specimen at any arbitrary rotation of the sample holder.

Returning to the issue of setting the sample and detector in the angular position necessary for the required measurement configuration, it can be formulated as follows: find a method to convert the set of input angles (θi, φi; θr, φr) specified by the user into a set of rotation angles (θz, θy; θx, ξ) to be executed by the available degrees of rotational freedom. This alignment aims to match the incident and scattered light beams specified in the sample reference frame S1 with the probe and detection frames defined in the laboratory reference frame S0, respectively.

Calculating these rotation angles is a fairly simple mathematical problem. However, the method for solving it, detailed in the next sections, will be useful for users intending to apply the gimbal-based SPS in their work.

3.2 Calculation of detection angle

In the case of TAMS, the spectrophotometer (1) emits the probe light beam and remains fixed in the laboratory reference frame, regardless of the selected measurement configuration.

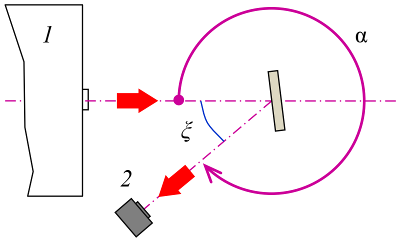

Figure 4. Convention for the definition of the detection angle

The detection angle (or, in other words, the angular position of the detector module (2)) in the Parameters Settings of the TAMS user interface should be set as follows (see Fig.4):

$$\alpha = 360° - \xi \tag{4}$$

The angle ξ can be easily derived from the dot product of unit vectors representing the propagation directions of incident rays (i) and scattered rays (r):

$$\cos\xi = \frac{\bar{i}\cdot\bar{r}}{\left\|\bar{i}\right\|\cdot\left\|\bar{r}\right\|} \tag{5}$$

From this equation, one can easily find that:

$$\cos\xi = \cos(\Delta\theta)\cdot\cos^2(\Delta\varphi/2) + \cos(\theta_i+\theta_r)\cdot\sin^2(\Delta\varphi/2) \tag{6}$$

, where $\Delta\varphi = \varphi_i - \varphi_r$ and $\Delta\theta = \theta_i - \theta_r$

3.3 Calculation of TAMS rotation angles

For a given set of input angles (θi, φi; θr, φr) for which BRDF measurement is needed, the angles of rotational displacements (θz, θy, θx) to be performed by the available rotation stages in order to move the sample from its initial position to the measurement position can be easily derived from the following matrix equation:

$$\mathbf{R}_{TAMS} = \mathbf{R} \tag{7}$$

In this equation, **R** is the rotation matrix, with elements determined by the chosen method of aligning incident and scattered beams with the probe and detection beams (see next section). $\mathbf{R}_{\mathrm{TAMS}}$ is also a rotation matrix, where the elements are defined by the available rotational degrees of freedom in the TAMS module.

It is instructive to note that R is a 3×3 constant matrix, while the elements of the $\mathbf{R}_{\mathrm{TAMS}}$ consist of trigonometric relationships involving three unknowns that need to be determined (rotation angles to be determined). In other words, the rotation angles specified in the TAMS controlling software can be easily obtained from a set of nine trigonometric equations.

3.4 Computing the rotation matrix $\mathbf{R}_{\mathrm{TAMS}}$

The rotation matrix $\mathbf{R}_{\mathrm{TAMS}}$, in the left-hand part of Eq. (7), is determined by the design used in the TAMS module rotation stages. More specifically, it can be expressed as the product of the rotation matrices corresponding to the degrees of rotational freedom offered by the sample holder module. In the case of the TAMS model employed in our work (Fig.2a), the rotation matrix $\mathbf{R}_{\mathrm{TAMS}}$ can be calculated using the following equation:

$$\mathbf{R}_{TAMS} = \mathbf{R}_{X''}\cdot\mathbf{R}_{Y}\cdot\mathbf{R}_{Z} \tag{8}$$

In this equation, the matrices $\mathbf{R}_{\mathrm{Z}}$, $\mathbf{R}_{\mathrm{Y}}$ and $\mathbf{R}_{\mathrm{X''}}$ define the rotations of the sample around the Z, Y and X″ axes by angles θ_z, θ_y and θ_x, respectively (see Fig.5).

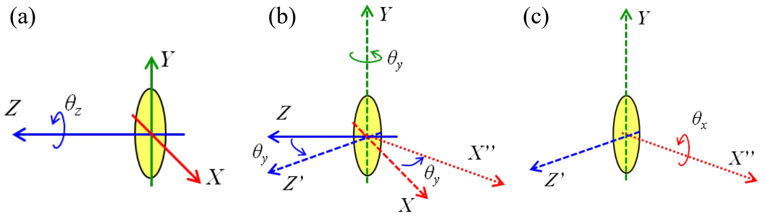

Figure 5 Schematic for three successive rotations of the sample around (a) Z-axis, (b) Y-axis and X″-axis

The rotation matrices $\mathbf{R}_{\mathrm{Z}}$ and $\mathbf{R}_{\mathrm{Y}}$ are determined as follows:

$$\mathbf{R}_z = \begin{bmatrix} c_z & -s_z & 0 \\ s_z & c_z & 0 \\ 0 & 0 & 1 \end{bmatrix} \tag{9}$$

$$\mathbf{R}_Y = \begin{bmatrix} c_y & 0 & s_y \\ 0 & 1 & 0 \\ -s_y & 0 & c_y \end{bmatrix} \tag{10}$$

In this and subsequent equations, the following notations are used to simplify their readability: $\cos\theta_i \rightarrow c_i$ and $\sin\theta_i \rightarrow s_i$.

Accordingly, the orientation of the rotation axis X″ can be found as follows:

$$\boldsymbol{X''} = \mathbf{R}_Y \cdot \begin{bmatrix} 1 \\ 0 \\ 0 \end{bmatrix} = \begin{bmatrix} c_y \\ 0 \\ -s_y \end{bmatrix} \tag{11}$$

It is straightforward to verify that $\|\mathbf{X}''\|=1$. Accordingly, the matrix of a rotation $\mathbf{R}_{X''}$ around the unit vector $\mathbf{X}''$ is given as:

$$\mathbf{R}_{x''} = \begin{bmatrix} c_y^2 + s_y^2 \cdot c_x & s_y \cdot s_x & -c_y \cdot s_y \cdot (1 - c_x) \\ -s_y \cdot s_x & c_x & -c_y \cdot s_x \\ -c_y \cdot s_y \cdot (1 - c_x) & c_y \cdot s_x & s_y^2 + c_y^2 \cdot c_x \end{bmatrix} \tag{12}$$

This expression can be easily obtained from the well-known formula for the matrix of a proper rotation by angle ε around an arbitrarily oriented in the space unit vector $\mathbf{u} = [u_1 \;\; u_2 \;\; u_3]^{\mathrm{T}}$:

$$\mathbf{R}_{\mathbf{u}} = \begin{pmatrix} u_1^2 + (1 - u_1^2) \cdot c\varepsilon & u_1 \cdot u_2 \cdot (1 - c\varepsilon) - u_3 \cdot s\varepsilon & u_1 \cdot u_3 \cdot (1 - c\varepsilon) + u_2 \cdot s\varepsilon \\ u_1 \cdot u_2 \cdot (1 - c\varepsilon) + u_3 \cdot s\varepsilon & u_2^2 + (1 - u_2^2) \cdot c\varepsilon & u_2 \cdot u_3 \cdot (1 - c\varepsilon) - u_1 \cdot s\varepsilon \\ u_1 \cdot u_3 \cdot (1 - c\varepsilon) - u_2 \cdot s\varepsilon & u_2 \cdot u_3 \cdot (1 - c\varepsilon) + u_1 \cdot s\varepsilon & u_3^2 + (1 - u_3^2) \cdot c\varepsilon \end{pmatrix} \tag{13}$$

Thus, we obtain:

$$\mathbf{R}_{TAMS} = \begin{bmatrix} c_y \cdot c_z + s_x \cdot s_y \cdot s_z & -c_y \cdot s_z + s_x \cdot s_y \cdot c_z & c_x \cdot s_y \\ c_x \cdot s_z & c_x \cdot c_z & -s_x \\ s_x \cdot c_y \cdot s_z - s_y \cdot c_z & s_y \cdot s_z + s_x \cdot c_y \cdot c_z & c_x \cdot c_y \end{bmatrix} \tag{14}$$

Finally, it is useful to note that in certain cases where both the incident and scattered beams are in the plane normal to the sample (i.e., $\varphi i = \varphi r \pm \pi$), BRDF measurements can be conducted using the TAMS module equipped with only one motorized rotation platform designed for rotations around the vertical Y-axis.
In these cases, the equations above can be rewritten as:

$$\mathbf{R}_{TAMS} = \mathbf{R}_Y \cdot \mathbf{R}_Z = \begin{bmatrix} c_y \cdot c_z & -c_y \cdot s_z & s_y \\ s_z & c_z & 0 \\ -s_y \cdot c_z & s_y \cdot s_z & c_y \end{bmatrix} \tag{15}$$

3.5 Computing the rotation matrix R

As noted above, the matrix **R** in the right-hand part of Eq. 7 is determined by the method used, or in other words, the algorithm for aligning the incident and scattered beams with the probe and detection beams. From basic mathematical considerations, it is evident that, in principle, it is possible to align two pairs of vectors using only one rotation around a unit vector whose direction can be derived from the set of input angles (θi, φi; θr, φr) and the direction angles of the probe and detection rays specified in the reference frames S1 and S0 (Fig.3). However, a more practical approach to solving the alignment problem is to employ iterative alignment methods, which involve at least two rotational displacements of the sample reference frame. In other words, one can decompose the matrix **R** into a set of matrices that are simpler to compute (each of these matrices is associated with a specific rotational displacement). In this paper, we specifically address the alignment method that involves only two successive rotations of the sample.

The first rotation is performed around the unit vector:

$$\overline{\mathbf{u}} = \frac{\overline{i} \times \overline{i_0}}{\left\| \overline{i} \times \overline{i_0} \right\|} = \begin{bmatrix} \sin\varphi_i \\ -\cos\varphi_i \\ 0 \end{bmatrix} \tag{16}$$

, where $\boldsymbol{i}_0 = [0 \;\; 0 \;\; 1]^{\mathrm{T}}$ and $\boldsymbol{i} = [\sin\theta_i \cdot \cos\varphi_i \;\; \sin\theta_i \cdot \sin\varphi_i \;\; \cos\theta_i]^{\mathrm{T}}$ are unit vectors associated with the light probe and incident beams, respectively (see Fig.3). It is clear that the unit vector $\boldsymbol{u}$ is orthogonal to both $\boldsymbol{i}_0$ and $\boldsymbol{i}$ vectors. Accordingly, a rotation of the sample frame by an angle $\theta_i = \mathrm{acos}(\boldsymbol{i_0} \cdot \boldsymbol{i})$ around the vector $\boldsymbol{u}$ aligns the vector $\boldsymbol{i}$ with the light probe beam. The rotation matrix corresponding to the first rotational displacement can be calculated as follows:

$$\mathbf{R}_1 = \begin{pmatrix} (s\varphi_i)^2 + (c\varphi_i)^2 \cdot c\theta_i & -s\varphi_i \cdot c\varphi_i \cdot (1 - c\theta_i) & -c\varphi_i \cdot s\theta_i \\ -s\varphi_i \cdot c\varphi_i \cdot (1 - c\theta_i) & (c\varphi_i)^2 + (s\varphi_i)^2 \cdot c\theta_i & -s\varphi_i \cdot s\theta_i \\ c\varphi_i \cdot s\theta_i & s\varphi_i \cdot s\theta_i & c\theta_i \end{pmatrix} \tag{17}$$

In this equation, the following notations are used to simplify its readability: *cos→c*, *sin→s*. The second rotational displacement of the sample frame is performed around the unit vector $\boldsymbol{i}$ obtained in the previous step (which is now parallel to the Z_0-axis; see Fig.3). This rotation of the sample frame aligns the unit vector **r'** associated with the scattered ray direction calculated after the first rotational displacement ($\mathbf{r'} = \mathbf{R}_1 \cdot \mathbf{r}$) with the unit vector $\mathbf{r}_0$ defining the direction of the detection ray in the laboratory reference frame (Fig.3).

The angle of rotation ε of the second rotational displacement can be calculated by two alternative methods, illustrated in Fig.6: either using the dot product of the projections of vectors **r'** and $\mathbf{r}_0$ on the plane β perpendicular to vector **i** around which the rotation is made ($\mathbf{r}_{0\beta}$ and $\mathbf{r}_\beta$, in Fig.6a), or using the one of vectors orthogonal to these projections ($\mathbf{V} \perp \mathbf{r}_{0\beta}$ and $\mathbf{V}_{\mathrm{target}} \perp \mathbf{r}_\beta$, in Fig.6b), as it was proposed in [18].

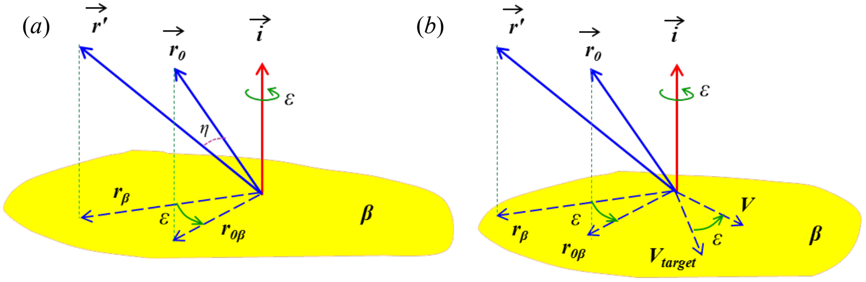

Figure 6. Schematic illustration of two methods used for calculating the rotation angle of the second rotational displacement of the sample frame: (a) the method using the projections of vectors **r'** and $\mathbf{r}_0$ and (b) the one involving vectors orthogonal to these projections

In this work, we use the former, the simplest method of calculation, in which the rotation angle ε (see Fig.6) is determined as follows:

$$\cos\varepsilon = \frac{\mathbf{r}_\beta \cdot \mathbf{r}_{0\beta}}{\|\mathbf{r}_\beta\| \cdot \|\mathbf{r}_{0\beta}\|} \tag{18}$$

In this equation: $\mathbf{r}_\beta = \mathbf{i} \times \mathbf{r'} \times \mathbf{i}$ and $\mathbf{r}_{0\beta} = \mathbf{i} \times \mathbf{r}_0 \times \mathbf{i}$, where $\mathbf{i} = [0\ \ 0\ \ 1]^{\mathrm{T}}$ and $\mathbf{r}_0 = [\sin\xi\ \ 0\ \ \cos\xi]^{\mathrm{T}}$ are respectively the unit vectors of incident and detection rays (specified in the frame S0).

It is instructive to note that applying Lagrange's formula to these vector triple products, it can be straightforwardly demonstrated that to obtain the Cartesian coordinates of the projections $\mathbf{r}_\beta$ and $\mathbf{r}_{0\beta}$ of vectors, we can just replace the z components of the vectors **r'** and $\mathbf{r}_0$ with zero (which can also be easily demonstrated from simple geometric considerations).

The rotation matrix corresponding to the second rotational displacement on the rotation angle ε can be calculated as follows:

$$\mathbf{R}_2 \equiv \mathbf{R}_z = \begin{bmatrix} \cos\varepsilon & -\sin\varepsilon & 0 \\ \sin\varepsilon & \cos\varepsilon & 0 \\ 0 & 0 & 1 \end{bmatrix} \tag{19}$$

Finally, the rotation matrix **R** corresponding to the used alignment method can be calculated as follows:

$$\mathbf{R} = \mathbf{R}_2 \cdot \mathbf{R}_1 \tag{20}$$

This 3×3 constant matrix can be easily calculated numerically. In our work, we use a very simple numerical model implemented in MATLAB programming environment.

Finally, it is important to note that the method for calculating the rotation matrix **R** presented in this article is certainly not the only one possible. For instance, in our work, we also developed an alternative method involving a sequence of three rotations of the angular bisector between the vectors corresponding to the incident and scattered light beams. This alternative calculation method is not included in this paper for the sake of brevity, and also because it yields the same results as the primary method discussed above in this subsection (which is quite expected and can be easily verified).

3.6 Computing TAMS angles

As noted above, the rotation angles (θ_z , θ_y , θ_x) of rotational displacements to be performed by available rotation stages to move the sample to the measurement position can be computed by equating each element in the obtained matrix **R** with the corresponding element in the matrix $\mathbf{R}_{\text{TAMS}}$ (see Eq.7), resulting in nine trigonometric equations. The periodic terms (such as ±kπ, ±2kπ …) in the solutions of these equations, corresponding to the number of complete revolutions of rotation stages, are of no practical interest, and there is no need to take them into account.

In addition, it is instructive to recall that, at oblique incidence, the probing and readout light spots projected on the sample surface have an elliptical shape. When the angles of incidence exceed a certain critical value, which in the case of the TAMS module is about 75°, the length of the major axis of the elliptical spots can become greater than the length or width of the sample under test, resulting in significant errors in the calculation of the BRDF. Accordingly, in practice, the rotation angles θ_y and θ_x (around the Y and X axes, respectively) should be chosen within the range of -75° to 75°.

Returning to the possible solutions of trigonometric equations derived from Eq.7, it is also worth noting that a given spatial orientation of the sample can always be achieved using more than one sequence of rotational displacements corresponding to available degrees of rotation freedom. This is schematically illustrated in Fig.7, which shows two ways to move the sample, represented by the letter "R", from an initial to a required position (indicated in Fig.7a as P_i and P_r, respectively).

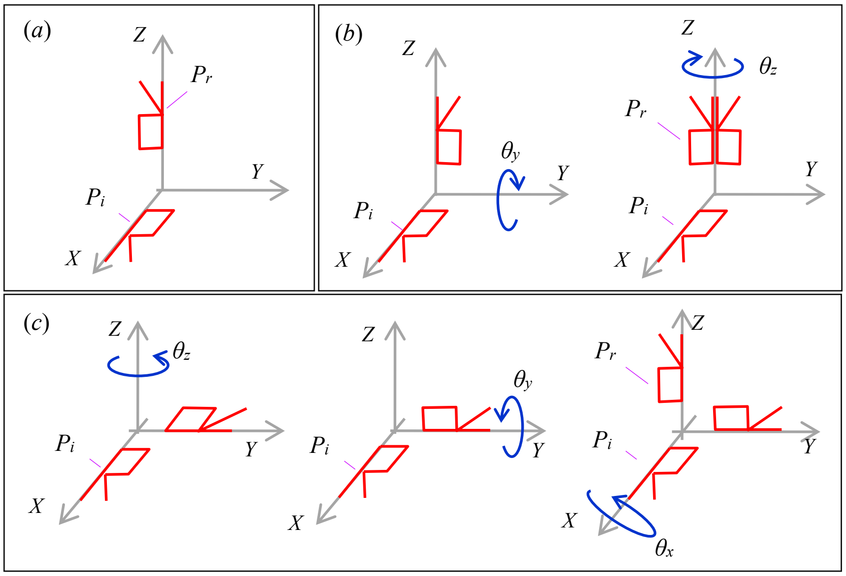

Figure 7. Schematic illustration of the multiplicity of possible solutions to the sample positioning problem

In the first case (Fig.7b), the rotations of the sample are performed in the following sequence: Y→Z→X and the rotation angles are (θ_z,, θ_y, θ_x) = ($-\pi$, $-\pi/2$, 0). In the second case (Fig.7c), the rotation sequence is Z→Y→X, and the rotation angles are (θ_z, θ_y, θ_x) = ($\pi/2$, $\pi/2$, $\pi/2$). Both these sequences of sample rotations are, of course, correct solutions to Eq.7 and provide the exact same final result but involve different times to complete the sample displacement procedure. On the other hand, since all components of the TAMS bench are stationary during the measurement of the sample BRDF, a comparative study of the dynamic behavior of and characteristics of the sample positioning system is currently of no practical interest to our work (although such study is of some academic interest). In other words, in our particular case, there is no principal difference in which solution of Eq.7 from among all possible ones to use to move the sample into the required angular configuration. Accordingly, in our experimental work, we limit ourselves to using only the following solution of this equation:

$$\theta_z = -a\cos\left(R_{22} \Big/ \sqrt{1-R_{23}^2}\right) \tag{21}$$

$$\theta_y = -a\cos\left(R_{33} \Big/ \sqrt{1-R_{23}^2}\right) \tag{22}$$

$$\theta_x = a\sin\left(-R_{23}\right) \tag{23}$$

Thus, the calculation of rotation angles (θ_z,, θ_y, θ_x) is a fairly simple numerical problem and can be performed in any user-accessible programming environment (in our work, as noted above, we use a numerical model written in MATLAB). It is important to note that when writing a numerical model, particular attention should be paid to the definition of rotation angle signs adopted in the software driver controlling motorized rotation stages of the TAMS ("TAMS Control" of OMT Solutions bv).

In the simplified model of the TAMS equipped only with one motorized rotation stage (Fig.2a), an alternative method of calculating the rotation angles (θ_z, θ_y) can also be used. However, as noted above, this model of the TAMS makes it possible to perform measurements of the sample BRDF only when both incident and scattered beams are in the same vertical plane (i.e., in the required angular configuration: $\varphi_i = \varphi_r \pm \pi$).
In this case, Eq.6 can be rewritten as:

$$\xi = \theta_i + \theta_r \tag{24}$$

Additionally, it is important to note that, in principle, the problem of aligning light beams can be addressed using the same method described above (i.e., involving Eq. 7). However, in the specific case where $\varphi i = \varphi r \pm \pi$, it can also be resolved in a much simpler manner through basic geometric considerations. The alternative alignment procedure consists of two successive rotations of the sample. The first rotational displacement of the sample frame is performed around the Z axis at an angle of $\theta z = \pi - \varphi i$. After this rotation, the plane formed by the incident and scattered beams coincides with the XZ plane, which contains the probe and detection beams. The second rotational displacement is executed around the Y axis at an angle of $\theta y = -\theta i$. Following this rotation, which completes the alignment of the two pairs of beams, the sample is positioned in the required angular configuration (θi, φi; θr, φr) for BRDF measurements.

It is instructive to note that it is quite easy to demonstrate that the matrix method involving Eq.7 and the alternative method, which is based on geometric considerations, give the same solution (θ_z,, θ_y). However, the latter method is very limited and can only be used in the case of the simplified model of the TAMS (see Fig.2a).

To conclude this section, it would be useful to discuss some aspects of the accuracy of the presented alignment method, more precisely, to evaluate the effect of the inaccuracies of the three rotation stages ($\delta\theta_z$ $\delta\theta_y$ $\delta\theta_x$) on the overall accuracy of the sample angular position adjustment.
In this context, it is instructive to note that, in the case of the TAMS currently used by us, the rotation around the axis Z (perpendicular to the sample surface) is performed manually, while the other two rotations are performed by motorized high-precision rotation stages. Accordingly, the contribution of the motorized rotation stage inaccuracy ($\delta\theta_y \approx \delta\theta_x \approx 0.02°$, see Table 1) to the overall angular positioning error of the sample can be considered negligible compared to that of the manual rotation stage (which, in the case of the manual rotation stage currently used in our measuring bench, is about $\delta\theta_z \approx 15$ mRad).
In practice, the precision of the sample angular positioning can be characterized using the error vector defined as:

$$\delta\boldsymbol{\varepsilon}_i = \mathbf{R}^{\delta}{}_{TAMS} \cdot \mathbf{i} - \mathbf{i} \tag{25}$$

, where $\mathbf{i}=[s\theta_i \cdot c\varphi_i \;\; s\theta_i \cdot s\varphi_i \;\; c\theta_i]^{\mathrm{T}}$ is the unit vector corresponding to the incident beam, and $\mathbf{R}^{\delta}{}_{TAMS}$ is an infinitesimal rotation matrix:

$$\mathbf{R}^{\delta}{}_{TAMS} = \begin{bmatrix} 1 & -\delta\theta_z & \delta\theta_y \\ \delta\theta_z & 1 & -\delta\theta_x \\ -\delta\theta_y & \delta\theta_x & 1 \end{bmatrix} \approx \begin{bmatrix} 1 & -\delta\theta_z & 0 \\ \delta\theta_z & 1 & 0 \\ 0 & 0 & 1 \end{bmatrix} \tag{26}$$

, which can be straightforwardly obtained by differentiating Eq.14 and subsequently suppressing infinitesimal second-order terms (keeping in mind also that, in our particular case: $\delta\theta_z >> \delta\theta_{x,y}$).
It is easy to see that the norm of the error vector, $\boldsymbol{\delta\varepsilon}_\mathrm{i}$, is equal to:

$$\left|\delta\boldsymbol{\varepsilon}_i\right| = \delta\theta_z \cdot \sin\theta_i \le \delta\theta_z \tag{27}$$

Accordingly, the angular uncertainty of the sample positioning performed using the available motorized sample holder, which should be taken into account further when considering the overall error budget of the measurement method, does not exceed $2\delta\theta_z$.

4. EXPERIMENTAL TESTS

4.1 Reference diffusers

It should be noted that many physical factors, such as stray-light-induced noise, can significantly affect the results of BRDF measurements. Assessing the impact of these factors on the measurement results is not trivial; solving this complex problem directly requires numerous auxiliary theoretical and experimental studies that address the individual contributions of each component of the optical characterization instrument to the total measurement error budget. However, implementing these studies is quite costly and time-consuming. The most effective way to eliminate systematic errors (bias) from the raw measurement data is to calibrate the optical bench using standard reference samples with known BRDF values, i.e., standard diffusers certified by independent national metrology standards laboratories.

In this work, we used two Lambertian-like diffusers, ‘white Zenith’ from Sphereoptics, as reference samples for calibrating the TAMS-based measurement bench and testing its operational functionality. These diffusers were previously characterized at the NIST (US National Institute of Standards and Technology) using the ROSI (Robotic Optical Scattering Instrument), at the PTB (Germany's national metrology institute ‘Physikalisch-Technische Bundesanstalt’), and finally, at the CSL on the robot-based high precision gonioreflectometer. The BRDF of each reference sample was measured in six different geometries. Table 2 presents some of the angular configurations and the spectral ranges for which calibration was performed by the aforementioned metrology laboratories.

Table 2. Measurement configurations involved in reference diffusers calibration certificates

Sample	**Measurement configuration** ***Name & angles*** (θ_i, φ_i; θ_r, φ_r)	**Spectral range** **(Metrology laboratory)**
#1	‘**METOGSE1**’ (38.5°, 45°; 52.5°, 225°)	400-2400 nm / **NIST** 400-2400 nm / **CSL**
	‘CO2M1’ (43°, 45°; 54°, 225°)	
	‘CO2M2’ (48°, 45°; 54°, 225°)	
	…	
#2	‘**METOGSE1**’ (38.5°, 45°; 52.5°, 225°)	400-1700 nm / **PTB** 400-2400 nm / **CSL**
	‘CO2M3’ (48.57°, 54.46°; 54°, 225°)	
	‘CO2M4’ (42.47°, 47.02°; 54.76°, -121.49°)	
	…	

The samples under test (1) are mounted with four pillar posts (2) on a base plate (3), as depicted in Fig.8. The height of the pillar posts 3 is adjusted to align the center of the sample front surface with the center of rotation of the motorized sample holder.

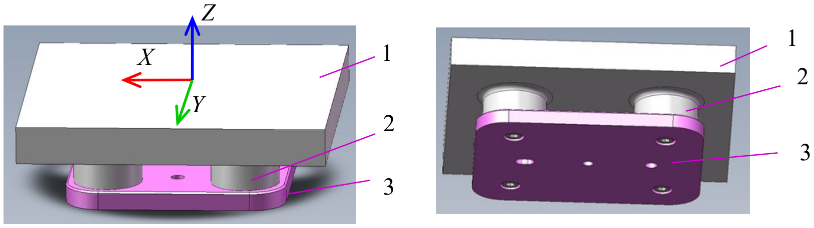

Figure 8. Mechanical layout of the sample assembly: top view (left) and bottom view (right)

To ensure reliable traceability of measurement results at different levels of metrological study, both reference diffusers have been characterized and certified, according to our test specification, for the same angular configuration, denoted in Table 2 as ‘METOGSE1’.

Table 3 presents the values and signs of the angles of rotational displacements to be executed by the TAMS motorized stages to position the sample in the necessary measurement configuration. These rotation angles are calculated using the developed rotation matrix method (see Eq. 4-23 above). The signs of the angles, which indicate the directions of rotation, are provided according to the sign convention utilized in the TAMS driver software.

Table 3. TAMS rotation angles calculated using the developed rotation matrix method

Measurement configuration	**TAMS angles**			
Name & angles (θ_i, φ_i; θ_r, φ_r)	θ_z	θ_y	θ_x	α
'**METOGSE1**' (38.5°, 45°; 52.5°, 225°)	-45°	-38.5°	0°	269°
'CO2M1' (43°, 45°; 54°, 225°)	-45°	-43°	0°	263°
'CO2M2' (48°, 45°; 54°, 225°)	-45°	-48°	0°	258°
'CO2M3' (48.57°, 54.46°; 54°, 225°)	-40.7°	-48.3°	5.9°	257.9°
'CO2M4' (42.47°, 47.02°; 54.76°, -121.49°)	-36°	-42.1°	-6.4°	263.4°

Finally, it is important to note that in our experimental work, we evaluate the error budget according to the standard methodology recommended by NIST [20]. For this reason, this paper omits details of the uncertainties analysis procedure for the sake of brevity, focusing only on the general results obtained (the main issues related to the uncertainties analysis problem will be published in a forthcoming paper).

4.2 Data processing method

Fig.9 shows a typical example of raw data obtained from the TAMS-based characterization bench when measuring the BRDF (in this example, for the reference diffuser #1).

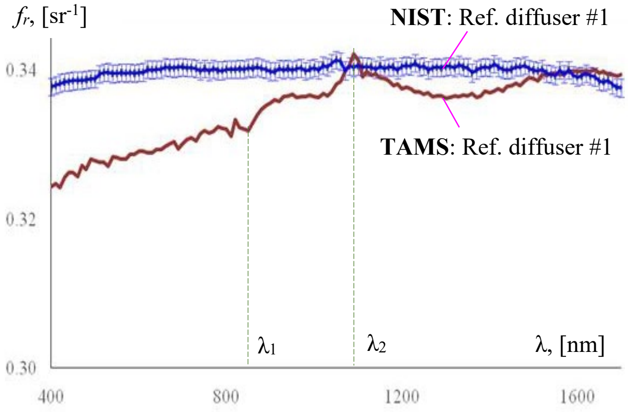

Figure 9. Example of the BRDF, fr, measuring raw data obtained from the TAMS-based measurement bench for reference diffuser #1. For comparison, the figure also shows the BRDF of the same sample measured by the NIST (with expanded uncertainties, k=2). In this example, for illustrative purposes only, the BRDF measured using the TAMS-based bench is presented without expanded uncertainty data (more detailed measurement information will be presented below). Two transition points on the graph of TAMS measuring results, λ1 = 860 nm and λ2 = 1100 nm, correspond respectively to switching the diffraction grating and changing the detector inside the used spectrophotometer, which is performed automatically during the spectral scanning.

As shown in Fig. 9, the relative error between the BRDF raw data obtained with the TAMS-based bench and the BRDF characterization data provided by NIST for the same reference sample remains below 4% and 1.2% in the wavelength ranges of 400-1100 nm and 1100-1700 nm, respectively.

Such a relatively small error, quite acceptable for many practical applications, cannot be considered acceptable in the case of reference diffusers dedicated to the spectral and radiometric calibration of on-board spectrometers. However, it should be noted that, as our experimental study has demonstrated, the discrepancy between these two data sets is clearly systematic rather than random (in other words, not related to detector noise or intrinsic noises of the used electronic hardware, etc.). Accordingly, it can be reduced by applying a calibration function $G(\theta i,\ \varphi i;\ \theta r,\ \varphi r;\ \lambda)$ to the raw measurement data, also called the 'correction factor function', which involves the BRDF of the reference sample measured with the TAMS bench normalized to the one provided by the NIST for the same angular configuration:

$$G(\theta_i,\phi_i;\theta_r,\phi_r;\lambda) = f\left(\left\langle BRDF_{TAMS}(\theta_i,\phi_i;\theta_r,\phi_r;\lambda)\right\rangle \big/ \left\langle BRDF_{NIST}(\theta_i,\phi_i;\theta_r,\phi_r;\lambda)\right\rangle\right) \tag{28}$$

It is important to note that this factor characterizes the response of the measuring instrument used and is largely independent of the optical response of the diffuser being measured.

The choice of data processing methods, particularly the correction of raw data, primarily depends on the research task at hand. In this context, it is important to note that in this paper, we consider only one research problem investigated in our current project: the extrapolation of BRDF data measured on robot-based gonioreflectometer benches (for example, on those of CSL or PTB) to the infrared wavelength range beyond the operating spectral ranges of these optical characterization benches. It is also worth mentioning that this problem is of significant practical interest, as TAMS-based characterization optical benches can theoretically be adapted to measure the BRDF of samples in the infrared spectral range up to wavelengths of 3 μm (i.e., the TAMS-based measurement setup covers a wavelength range much wider than other currently available measuring instruments, see Table 2).

The approach to solving the problem of extrapolation/interpolation proposed and examined in our work consists of the following general steps:

1) Calculating the relative spectral response functions (RSRFs; see Eq. 3) from BRDF measurement data available for the reference sample (NIST and TAMS data) and for the diffuser under test (DUT), which requires data extrapolation and/or interpolation. It is important to note that we work with two sets of data for the DUT: the measurement data that needs to be extrapolated (interpolated) and the uncalibrated measurement data obtained with the TAMS bench.
2) Calculating the correction factor function $G_\psi(\theta_i, \varphi_i; \theta_r, \varphi_r; \lambda)$ using the RSRFs calculated in the previous step for the reference sample (i.e., NIST and TAMS measurement data). The calculation is performed using the following equation:

$$G_\psi(\theta_i,\phi_i;\theta_r,\phi_r;\lambda) = \psi_{TAMS}(\theta_i,\phi_i;\theta_r,\phi_r;\lambda) \big/ \psi_{NIST}(\theta_i,\phi_i;\theta_r,\phi_r;\lambda) \tag{29}$$

3) Applying this correction factor function to the RSRF $\Psi_{TAMS,\,DUT}(\theta_i, \varphi_i; \theta_r, \varphi_r; \lambda)$ corresponding to the TAMS data of the DUT:

$$\psi_{DUT}(\theta_i,\phi_i;\theta_r,\phi_r;\lambda) = \psi_{TAMS,DUT}(\theta_i,\phi_i;\theta_r,\phi_r;\lambda) \big/ G_\psi(\theta_i,\phi_i;\theta_r,\phi_r;\lambda) \tag{30}$$

4) Fitting the obtained RSRF $\Psi_{DUT}(\theta_i, \varphi_i; \theta_r, \varphi_r; \lambda)$ to the RSRF calculated (using Eq. 30) for the DUT measurement data allows for extrapolation or interpolation. The primary objective of the fitting procedure is to minimize the scale difference between these two RSRFs within the spectral range where measurement data are available for both functions. The extrapolated part of the RSRF is the portion that results from fitting and falls within the spectral range not covered by the available DUT measurement data.
5) Calculating the absolute BRDF data for extrapolated/interpolated part $\Psi_{ext/int}(\theta_i, \varphi_i; \theta_r, \varphi_r; \lambda)$ of the RSRF spectral curve (if required). This conversion can be performed using the following equation (straightforwardly obtained from the rule of three):

$$BRDF(\theta_i,\phi_i;\theta_r,\phi_r;\lambda) = \Psi_{\mathrm{ext/int}}(\theta_i,\phi_i,\theta_r,\phi_r,\lambda) \cdot \left\langle\left\langle BRDF(\theta_i,\phi_i,\theta_r,\phi_r,\lambda)\right\rangle\right\rangle_\lambda \tag{31}$$

In this equation, the $<<BRDF(\theta_i, \varphi_i; \theta_r, \varphi_r, \lambda)>>_\lambda$ is averaged spectral value of the DUT BRDF, used in step #1 of this method, to convert the absolute BRDF of the DUT into its RSRF.

In our work, we tested the proposed method of data processing to solve the following two problems (discussed below for illustration purposes): (1) extrapolating the PTB measurement data and (2) extrapolating/interpolating the BRDF data obtained on the CSL robot-based gonioreflectometer bench. Solving these problems not only illustrates the basic idea of the proposed data processing method but also represents significant practical interest for our current project.

Regarding the former problem, as noted above, the PTB measures the BRDF over a relatively narrow wavelength range compared to NIST and CSL (see Table 2). Consequently, this issue involves estimating the BRDF values of reference diffuser #2 in the wavelength range from 1700 nm to 2400 nm, which is not covered by the PTB calibration certificate. As explained earlier, the estimation procedure entails the correction factor function $G\psi(\theta i, \varphi i; \theta r, \varphi r; \lambda)$, calculated from the BRDF data provided by NIST and acquired using the TAMS measuring bench for reference diffuser #1 (cf. Eq.29).

Fig. 10 displays the plots of the NIST and TAMS relative spectral response functions for reference diffuser #1, along with the corresponding correction factor function calculated for the METOGSE1 angular configuration (see Table 2).

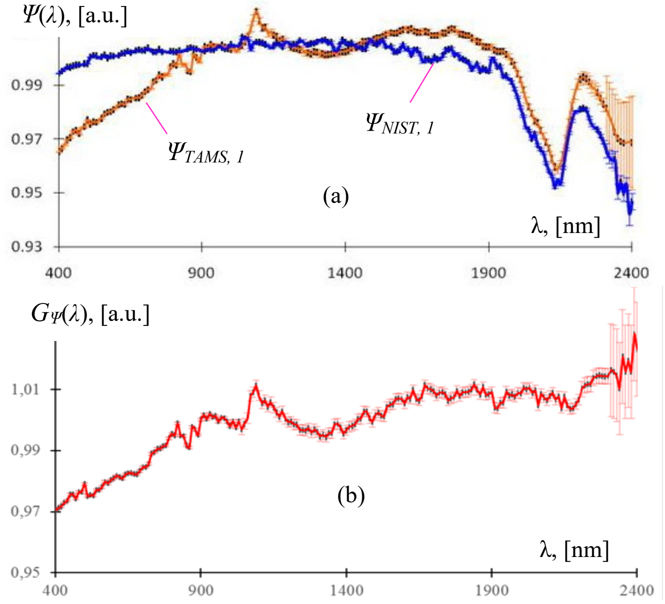

Figure 10. Calculation results obtained at steps #1 and #2 of the proposed data processing method: (a) RSRFs of the reference diffuser #1 calculated for the METOGSE1 angular configuration from the BRDF data provided by NIST ($\Psi_{NIST,1}$) and from the ones measured with the TAMS setup ($\Psi_{TAMS,1}$); (b) the correction factor function $G_\psi(\lambda)$ calculated with Eq.29 for these RSRF data.

As mentioned above, in this work, the measurement results are analyzed in terms of the RSRFs, defined by Eq.3. In other words, the data processing method used involves normalizing the raw spectral data. This approach is well-suited for comparative studies, as the normalization significantly reduces scale differences between the spectra being compared, which arise principally from differences in measurement conditions [21]-[22]. This greatly facilitates the recognition and tracking of specific features in the measured scattering spectra, indicating differences in the optical properties of the samples under test.

Fig. 11 presents an example of a comparative analysis of measurement results illustrating the practical benefits offered by this approach.

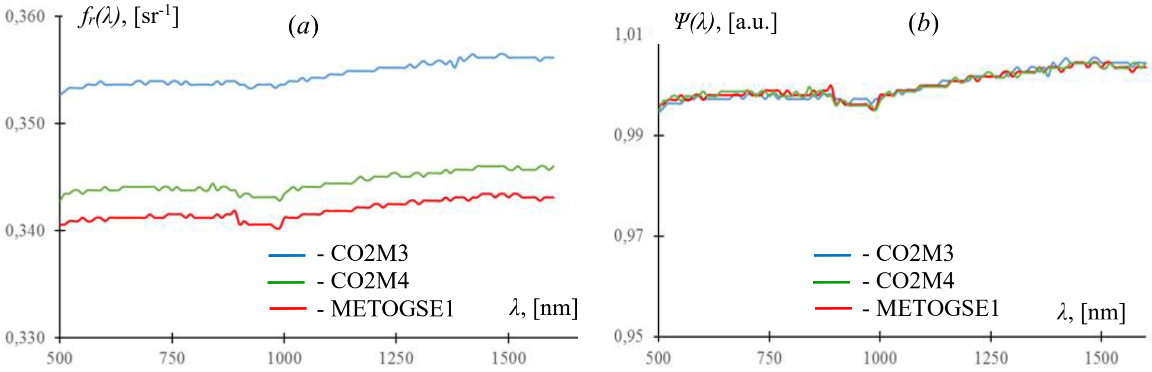

Figure 11. (a) BRDFs of the reference diffuser #2 measured for three angular configurations (see Table 2); (b) corresponding RSRFs (i.e., the identical spectra after applying the normalization rule defined by Eq.3)

In this figure, for illustrative purposes, only three measured spectra are presented. However, in practice, the experimental results typically contain several series of measurement data, each of which may include up to several dozen measured spectra that are slightly shifted vertically from one another. This results in continuous bands of curves on the graph, which greatly complicates the correct interpretation and understanding of the measurement results. After normalization, the spectral curves (RSRF) overlap, making specific features more noticeable (such as local oscillations in the spectral range of 800-1150 nm, see Fig. 11b). These features are not associated with random measurement errors and are therefore of interest for further detailed study.

Regarding the curve fitting procedure conducted in step #4 of the proposed data processing methodology, it utilizes the well-known least squares method. This method involves determining a correction factor by which the RSRF predicted for reference diffuser #2 using Eq.30 should be multiplied to eliminate the scale difference between the corrected RSRF and the RSRF derived for the same sample from PTB measurement data in the spectral band of 400-1700 nm (where both RSRFs can be determined simultaneously, see Table 2).

It is instructive to note that, in the case of the spectrophotometer used in this work (UV/Vis/NIR PerkinElmer LAMBDA™ 1050), the scanned wavelength range (400-2400 nm) consists of three independent spectral bands: 400-860 nm, 860-1100 nm, and 1100-2400 nm (or 1100-1700 nm when the purpose of the study is to compare TAMS data with PTB reference data). These bands are delimited by two transition points, λ_1= 860 nm and λ_2=1100 nm, which correspond to the diffraction grating switching and the automatic change of the detector during the spectral scanning, respectively. Thus, from a functional perspective, the measurement data obtained with this spectrophotometer can be considered as derived from three virtual spectrophotometers operating independently in these spectral bands. Therefore, the estimated RSRF curve $\Psi_{DUT}(\lambda)$ can be viewed as a superposition of three independent parts. Consequently, the data fitting can be performed independently in these three spectral bands, and the resulting correction factor values may differ slightly for each band. Regarding the part of the spectral range in which the RSRF is extrapolated (i.e., 1700-2400 nm), the correction factor applied to the RSRF calculated using Eq.30 is assumed to be equal to that obtained for the spectral band 1100-1700 nm.

The calculation results obtained using the proposed data processing method are presented in Fig. 12.

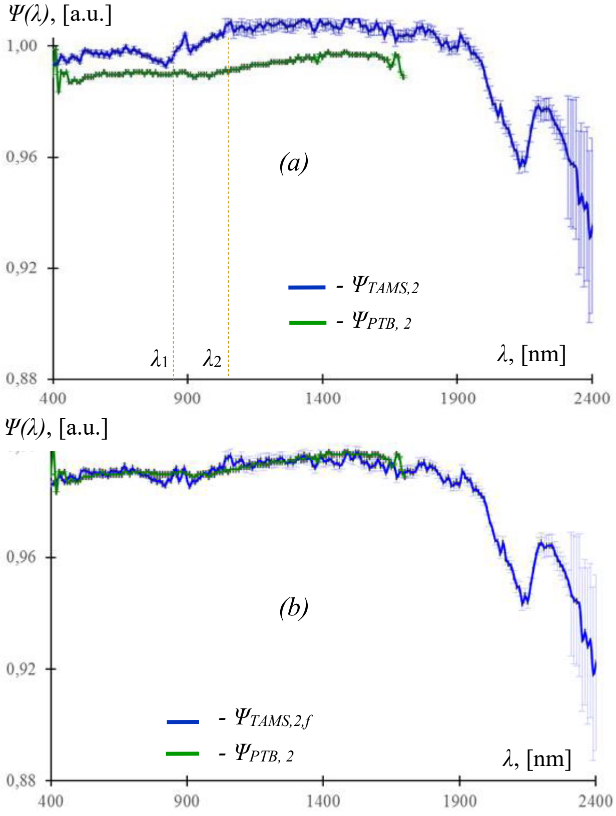

Figure 12. Calculation results obtained at steps #3 and #4 of the proposed data processing method: (a) the RSRF of the reference diffuser #2 calculated for the METOGSE1 angular configuration from the BRDF data provided by PTB ($\Psi_{PTB,2}$) and the RSRF of the same diffuser ($\Psi_{TAMS,2}$) obtained by applying the correction factor $G_{\psi}(\lambda)$, calculated in the previous step #2 (see Fig.10b), to the RSRF evaluated from the BRDF data measured with the TAMS setup; (b) RSRF data from the curve correction procedure performed in step #4 of the proposed method.

As shown in Fig. 12a, the RSRF spectra display significant spurious oscillations near the boundary wavelengths of the operational spectral ranges (i.e., around λ = 860 nm for TAMS RSRF data, as well as λ = 400 nm and λ = 1700 nm for PTB RSRF data). These transient oscillations are less related to the optical response of the sample under test and more to a decrease in the efficiency of the diffraction grating used in the TAMS spectrophotometer or in the monochromator, in the case of the gonioreflectometer. Furthermore, since least-squares analysis is highly sensitive to outliers, these oscillations can considerably skew the results of the curve-fitting procedure based on this method. Therefore, to minimize the effect of these oscillations on the curve-fitting results, the RSRF data in the relevant spectral bands are excluded from consideration when calculating the correction factor (i.e., in step #4 of the proposed data processing).

In the spectral band 2300-2400 nm (Fig.12), the measurement uncertainty exceeds the tolerance limits established by the technical specification for the application under consideration (i.e., the development and metrology of reference diffusers dedicated to on-board calibration units of space spectroscopic instruments) while remaining quite acceptable for many other practical applications.

Although the sources of the statistically significant increase in measurement uncertainties observed in the wavelength band of 2300-2400 nm are still under investigation, it is clear that the contribution of uncertainties originating from the measurement bench itself (for example, related to the spectrophotometer drift, stray light, etc.) to the total error budget in this range is too small to explain the observed increase in uncertainty levels. The validity of this assumption is well supported by our experience with the spectrophotometer used in the TAMS measuring bench, gained through work on numerous spectroscopic applications. Accordingly, the most likely sources of the observed increase in measurement uncertainties in the spectral band 2300-2400 nm are related to the design of the sample holder assembly. The design optimization of this assembly is currently in progress; a specific paper with detailed explanations of the results of this work will be published in the near future.

As noted above, the current version of the fitting procedure employs the well-known least squares method (LSM), which involves minimizing the sum of squares of residuals (SSR). In our case, this represents the deviation of RSRF values predicted for reference diffuser #2 from the RSRF derived from PTB measurement data. However, it should be noted that this approach is not the only one possible. For instance, an alternative fitting procedure could be developed where the objective function to minimize is based on the number of points that do not meet an accepted criterion for compliance with the specification. It may be recalled that compliance with the specification is typically considered achieved if the measured result, extended by the expanded uncertainty interval at the 95% confidence level, does not exceed the tolerance limits defined in the specification (for a more detailed explanation, see [23] "Appendix B. Assessment of Compliance with Specification"). It is instructive to note that the fitting analysis involving the mentioned compliance criterion can be used in combination with conventional LSM.

This alternative approach to curve fitting is still under development because its practical implementation requires a substantial reduction in measurement uncertainties and, consequently, further optimization of the TAMS setup design and the measurement methodology.

Finally, concerning step #5 of the proposed data processing method, as previously mentioned, the RSRF obtained after fitting in step #4 is converted to the absolute BRDF using the same conversion factor applied to calculate the PTB RSRF in step #1 of this data processing method (i.e., the averaged spectral value of the PTB BRDF; see Eq.31).

The calculation results obtained after applying the conversion rule defined by Eq.31 are shown in Fig.13.

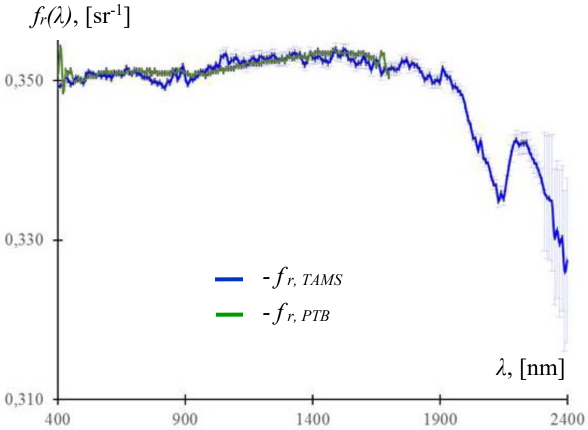

Figure 13. Calculation results obtained at the step #5 of the proposed data processing method: $f_{r,\ PTB}$ - the BRDF data provided for the reference diffuser #2 by PTB (the METOGSE1 measurement configuration) and the BRDF of the same diffuser ($f_{r,\ TAMS}$), calculated at the step #5 of the proposed data processing method

To conclude, it seems reasonable to construct the absolute BRDF of reference diffuser #2, which will be used in upcoming data processing and calibration procedures as global reference data, by combining the available PTB data for the spectral range of 450-1660 nm with the BRDF obtained by extrapolating TAMS data available for the spectral bands of 400-450 nm and 1660-2300 nm. As explained above, the spurious oscillations observed near the boundaries of the PTB operational spectral ranges, specifically near the wavelengths λ= 400 nm and λ= 1700 nm, are unrelated to the optical response of the diffuser under test. Therefore, the PTB BRDF data in the corresponding spectral bands, 400-450 nm and 1660-1700 nm, should be replaced by the corresponding TAMS data.

Returning to the second example application of the proposed data processing approach, it is important to note that although the objectives and conditions we address are slightly different from those in the first example considered, the overall methodology for solving it remains consistent. Therefore, in this subsection, only the most significant issues related to this problem and the final results of data processing are discussed.

As noted above, in the second example, the proposed data processing method is utilized to extrapolate and interpolate BRDF data previously obtained using the CSL robot-based gonioreflectometer bench.

In this example, the sample under test is a polytetrafluoroethylene (PTFE)-based diffuser. The BRDF of the sample was measured using the CSL robot-based gonioreflectometer in the angular configuration 'METOGSE1' (see Table 2) for eleven wavelengths selected in the spectral range from 445 nm to 2250 nm (detailed explanations of the operational principle and performance parameters of this measuring bench can be found in our previous publications [18]-[19]).

Fig. 14 presents the results of measuring the BRDF of the PTFE sample conducted with the CSL robot-based gonioreflectometer, alongside the BRDF of the same sample calculated from TAMS measurement data using the proposed data processing method.

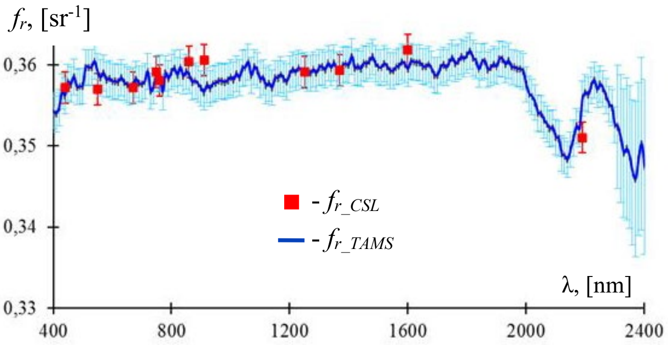

Figure 14. BRDF measured with the CSL robot-based gonioreflectometer (f_{r_CSL}) and the one calculated TAMS from TAMS measurement data using the proposed data processing method (f_{r_TAMS}). An offset is applied on gimbal data, to match the median of robot-based results.

Fig. 14 reveals a relatively good agreement between the BRDF data obtained using the two aforementioned measurement methods: the relative spectral difference between the two measurements is within ±0.6% over the spectral range of interest from 400 nm to 2300 nm and does not exceed ±1% at wavelengths 865 nm and 913 nm. Accordingly, one can conclude that the investigated instrumental approach, involving the TAMS bench and the proposed data processing methodology, provides measurement accuracy comparable to that achievable with the robot-based gonioreflectometer. This makes the approach well-suited for implementing the aforementioned cost-effective sample characterization strategy.

In conclusion, it would be informative to briefly discuss how the stability of the measuring system over time affects measurement precision.

As noted above, the measurement system used in our work is based on the PerkinElmer LAMBDA™ 1050 UV/Vis/NIR spectrophotometer equipped with the TAMS module. Despite the high performance and accuracy of this instrument, prolonged measurements can introduce internal uncertainties primarily due to stray light, residual variations in the intensity of the illuminating beam, noise in the detectors, and the readout electronics, potentially leading to unacceptably high measurement errors. Therefore, special attention must be given to stability issues and the appropriate selection of spectral scanning parameters that affect the total duration of measurements (such as integration time, wavelength step, spectral range width, etc.).

As our experience has shown, achieving the necessary precision and repeatability of measurements for our metrological application requires careful selection of the spectral scanning parameter values. These values must ensure that the total duration of the BRDF measurement procedure, which involves, as explained above, two consecutive measurements of the intensity spectra of the reference and scattered beams, does not exceed 12 hours. This guideline for selecting spectral scanning parameters is, of course, purely indicative. The maximum duration for measurements was established experimentally and mainly depends on the performance characteristics of the spectrophotometer used in experimental work.

5. CONCLUSION

In this paper, we present an innovative and cost-effective approach to BRDF metrology, which includes an instrumental platform paired with an appropriate data processing method. The instrumental platform, specifically its initial proof-of-concept prototype, was developed based on the commercially available standard spectrophotometer PerkinElmer LAMBDA™ 950/1050, which is equipped with a sample positioning system (SPS) that utilizes a compact motorized gimbal. Our gimbal-based SPS, which is of our own design, is currently under development. Consequently, the first prototype of the measurement bench incorporates an SPS built around the commercially available TAMS module, which has been slightly modified to enable BRDF measurements in an arbitrary angular configuration of the samples (an additional rotation stage has been added to the sample holder). This instrumental approach complements existing robot-based BRDF measurement benches and is intended for conducting metrological tests on small, lightweight samples, primarily for intermediate characterization of samples between non-critical process operations. We discuss several key engineering aspects of the practical implementation of the proposed instrumental approach. The functionality of the developed characterization bench was tested through tasks involving the interpolation and extrapolation of BRDF measurement data obtained with the CSL robot-based gonioreflectometer.

The proposed instrumental approach is well-suited for small research laboratories since its practical implementation does not require significant expenses compared to robot-based gonioreflectometers or adapted large clean rooms. One of the main advantages of this approach is its high flexibility for scheduling metrological test research. Finally, the relatively small size of the measuring bench facilitates the implementation of BRDF measurements in a dry nitrogen-purged environment, thus preventing the effect of light absorption by water vapor when measuring in the infrared range.

ACKNOWLEDGEMENTS

This research has been performed in the frame of a contract between CSL and Thales Alenia Space France for the design and development of the CO2I Flight Calibration Unit, in the frame of the ESA Copernicus CO2M Mission, funded by the EU and ESA.

REFERENCES

[1] Stover, J., "Optical Scattering: Measurement and Analysis", SPIE press book (2012)

[2] Domken I., Plesseria J.-Y. and Mazy E., “MSI Instrument (ESA Sentinel-2): from the diffuser procurement until the test instrument at CSL”, 26th Aerospace Testing Seminar, (2011)

[3] Mazy E., Camus F. and Chorvalli V., “Sentinel-2 diffuser on-ground calibration”, Proc. SPIE 8889 (2013)

[4] Clermont L., Mazy E., Marquet B., Plesseria, JY., “An in-flight calibration for the Earth observation instrument Sentinel-4: from design to tests”, Proc. SPIE 11116 (2019)

[5] Clermont, L. et al., "Design and tests of the sun baffle for the Sentinel-4 UVN embedded calibration assembly", Proc. SPIE 10562, International Conference on Space Optics — ICSO 2016, 1056201 (25 September 2017)

[6] Plesseria, J.Y., et al., "Utilisation of acktar black coatings in space applications," International Symposium on Materials in the Space Environment (2018).

[7] Clermont, L., "Stray light control in off-axis three mirrors anastigmats for earth observation", Proc. SPIE 11852, International Conference on Space Optics — ICSO 2020, 118524X (11 June 2021); https://doi.org/10.1117/12.2599819

[8] Clermont, L, Aballea, L., "Stray light control and analysis for an off-axis three-mirror anastigmat telescope," Optical Engineering 60(5), 055106 (28 May 2021). https://doi.org/10.1117/1.OE.60.5.055106

[9] Clermont, L., Lallemand, E., Plesseria, J. Y., Serrano, S., and Kintziger, C., "The stray light baffle for the ARRAKIHS mission", Proc. SPIE 13092, Space Telescopes and Instrumentation 2024: Optical, Infrared, and Millimeter Wave, 130923O (23 August 2024); https://doi.org/10.1117/12.3021043

[10] J. Moreno-Ventas, W. Moelans, A. Mazzoli, L. Aballea, P. Blain, E. Mazy, L. Clermont, N. Saillen, L. Montrone, and M. Francois "ALTIUS instrument: a study of scattering effects", Proc. SPIE 12777, International Conference on Space Optics — ICSO 2022, 127771N (12 July 2023); https://doi.org/10.1117/12.2689672

[11] Clermont, L., C.Michel, Chouffart, Q. et al. Going beyond hardware limitations with advanced stray light calibration for the Metop-3MI space instrument. Sci Rep 14, 19490 (2024). https://doi.org/10.1038/s41598-024-68802-z

[12] Clermont, L.; Michel, C.; Stockman, Y. Stray Light Correction Algorithm for High Performance Optical Instruments: The Case of Metop-3MI. Remote Sens. 2022, 14, 1354. https://doi.org/10.3390/rs14061354

[13] Clermont, L., Michel, C., Mazy, E., Pachot, C., Daddi, N., Mastrandread, C., and Stockman, Y., "Stray-light calibration and correction for the MetOp-SG 3MI mission", Proc. SPIE 10704, Observatory Operations: Strategies, Processes, and Systems VII, 1070406 (10 July 2018); https://doi.org/10.1117/12.2314208

[14] Clermont, L, Michel, C., "Out-of-field stray light correction in optical instruments: the case of Metop-3MI," Journal of Applied Remote Sensing 18(1), 016508 (4 March 2024). https://doi.org/10.1117/1.JRS.18.016508

[15] A. Hoepe et al., “Robot-based gonioreflectometer”, Industrial Robotics: Programming, Simulation and Application, ISBN 3-86611-286-6, ARS/plV, Germany, IntechOpen (2006)

[16] H.J. Patrick et al., “Bidirectional reflectance capabilities of the NIST Robotic Opticall Scattering Instrument”, Appl Opt. **60**/28 (2021)

[17] J.-Y. Plesseria, I. Domken, E. Mazy et al., “Development of a BRDF Measurement Bench for Characterization of Diffuse Reflective Materials”, Proceedings of 12th European Conference on Spacecraft Structures, Materials and Environmental Testing (2012)

[18] Clermont, L., Michel, C., and Mazy, E., “Performance enhancement of a BSDF test bench using an algorithm fed with laser-tracker measurements”. Proceedings of SPIE: The International Society for Optical Engineering, 11057 (2019)

[19] E. Mazy, C. Michel, S. Marcotte, L. Clermont, B. Marquet, J. Jacobs, I. Domken, and Y. Stockman "Recent development in BTDF/BRDF metrology on large-scale Lambertian-like diffusers: application to on-board calibration units in space instrumentation", Proc. SPIE 11102, Applied Optical Metrology III, 1110204 (12 September 2019); https://doi.org/10.1117/12.2529542

[20] B.N. Taylor and Ch. E. Kuyatt, “Guidelines for Evaluating and Expressing the Uncertainty of NIST Measurement Results”, NIST Technical Note 1297, 1994 Edition, NIST, National Institute of Standards and Technology, (1994)

[21] A. Rinnan et al., “Data pre-processing”, Infrared Spectroscopy for Food Quality Analysis and Control, Elsevier Inc. (2009)

[22] T.W. Randolph, “Scale-based normalization of spectral data”, Cancer Biomark (2006)

[23] K. Birch, “Measurement Good Practice Guide No. 36. Estimating uncertainties in testing”, British Measurement and Testing Association, UK, (2003)